Received: 4 December 2020 | Revised: 13 February 2021 | Accepted: 19 February 2021

DOI: 10.1002/nano.202000271

RESEARCH ARTICLE

Nano Select Open Access WILEY

Near-infrared responsive targeted drug delivery system that offer chemo-photothermal therapy against bacterial infection

Unnati Patel[1] | **Kavini Rathnayake**[1] | **Hemang Jani**[2] | **Kalana W. Jayawardana**[3] | **Rijan Dhakal**[1] | **Lingze Duan**[2] | **Surangi N. Jayawardena**[1]

[1] Department of Chemistry, The University of Alabama in Huntsville, Huntsville, Alabama 35899, USA

[2] Department of Physics, The University of Alabama in Huntsville, Huntsville, Alabama 35899, USA

[3] Department of Biomedical Engineering, Vanderbilt University, Nashville, Tennessee 37235, USA

Correspondence
Surangi N. Jayawardena, Department of Chemistry, The University of Alabama in Huntsville, Huntsville, AL 35899, USA.
Email: hj0022@uah.edu

Funding information
University of Alabama in Huntsville

Abstract

To combat the rise of antibiotic resistant bacteria, it is essential to look upon other therapeutic solutions that do not solely depend upon conventional antibiotics. Here, we have designed a combinational therapeutic approach that kills bacteria with the conjunction of photothermal (PT) and antibiotic therapy. A near-infrared (NIR) laser activated targeted drug delivery nano-assembly delivers antibiotic as well as offer PT therapy (PTT). The synergistic application of both therapies increases the efficacy of treatment. The protected delivery of antibiotic and its release in the proximity of the bacteria surface reduces off-target toxicity and reduce the efficacious dosage. Core of the nano-assembly is composed of NIR active gold nanorods (GNRs) coated with a mesoporous silica nanoparticle (MSNP), which serves as a carrier for an anti-tuberculosis drug bedaquiline (BDQ). The assembly was wrapped within a thermo-sensitive liposome (TSL) conjugated to mycobacteria-targeting peptide: NZX, GNR@MSNP@BDQ@TSL@NZX. NZX mediates adhesion of final nano-assembly on mycobacteria surface. Upon NIR laser irradiation GNRs convert photo energy of the laser to localized heat, which melts TSL triggering release of BDQ. Antibacterial activity of final nano-assembly against *Mycobacterium smegmatis* (*Msmeg)* was 20 folds more efficacious than the free drug equivalent. The final nano-assembly could also successfully inhibit the growth of intracellular mycobacteria residing in lung cells.

KEYWORDS
gold nanorods, intracellular bacteria, nano-assembly, photothermal therapy, targeted drug delivery, thermo-sensitive liposomes

1 | INTRODUCTION

Antibacterial resistance is a major global health concern, with new antibacterial resistant strains appear at an alarming rate.[1] Multi-drug resistant (MDR) bacterial infections have caused 2.8 million infections and 35,000 deaths in United States in the past few years.[1] New therapeutic options are required to combat this increasing problem.[2,3] Targeted drug delivery is an attractive alternative to traditional oral broad-spectrum non-targeted small molecule antibiotics.[4,5] But even with cutting-edge antibiotic delivery strategies, antibacterial activity still relies upon on the therapeutic efficacy of the encapsulated drug. Combination therapy combining an antibiotic with a different modality of treatment such as photothermal (PT), magnetothermal therapies have recently emerged to the surface of other opional antibacterial therapies.[6–9] Here, we have designed a targeted antibiotic delivering nano-assembly that exerts chemo-photothermal therapy (chemo-PTT). This combined therapeutic approach has higher therapeutic efficacy than the lone antibiotic. Our nano-assembly is an engineered core-shell particle, consisting of drug entrapped photosensitive core and a stimuli responsive shell. This engineered nano-assembly has the following features: (1) synergistic antibacterial activity due to encapsulated small molecule antibiotic and photothermal (PT) activity (2) targeted antibiotic delivery to bacteria cell surface which reduce off-target toxicity (3) remote trigger release of encapsulated antibiotics upon exposure to near-infrared (NIR) laser.

Among available nanoplatforms, gold nanoplatforms are used most extensively in PTT. These include gold nanospheres, nanorods (GNRs),[10,11] nanocages,[12] nanoshells,[13,14] nanostars[15] and all have been successfully used both in-vitro and in-vivo. GNRs exhibits strong longitudinal absorbance at the NIR I window of 700-1000 nm with excellent application in the photo-induced therapies.[16] Additionally, by adjusting aspect ratios, GNRs can easily attenuate a strong absorption at particular wavelength.[17] Therefore, GNRs were used in the nano-assembly to absorb NIR light and generate PT activity. GNRs were coated in a mesoporous silica shell (GNR@MSNP) to improve drug loading capability. Porous inorganic shells are widely used in drug delivery applications due to their large pore volume, pore size and surface area.[18–22] Therefore, drug (bedaquiline, BDQ) was loaded into mesoporous silica shell containing GNR@MSNP (GNR@MSNP@BDQ). This was then encapsulated in a thermally-sensitive liposome (TSL, GNR@MSNP@BDQ@TSL). Liposome encapsulation offer controlled release of drug and prevents premature release before the nano-assembly approaches the target.[23,24] The selected drug BDQ is a novel antibacterial therapeutic against tuberculosis (TB). Heat generated from the GNRs upon NIR exposure cause the TSL to undergo a phase transition and become permeable, releasing encapsulated BDQ. Exposure to NIR laser generates hyperthermia which can lead to the permeability in bacterial cell membrane, cause leakage of bacterial cell content and subsequent bacterial cell death.[25] To guide the liposome to the mycobacteria surface, mycobacteria recognizing antibacterial peptide NZX was used.[26] Antibacterial peptide was used as a targeting ligand as it can also exert a degree of antibacterial activity, and therefore far more attractive than other biomarker targeting ligands.[27] With the addition of NZX the final nano-assembly was abbreviated as GNR@MSNP@BDQ@TSL@NZX.

Other studies have also used similar combination therapy approaches combining PTT and antibiotic therapy to combat bacterial infections.[6,28,29] Recent work done by Quing et al. reported combined chemo-PTT nanostructure against methicillin-resistant *Staphylococcus aureus* (MRSA) bacterial infection.[5] Ma et al. also reported combining strategies for chemo-PTT therapy against *Escherichia coli* and *Staphylococcus aureus*.[30] Both reported combinational therapies against bacteria lack the targeting ability of nanomaterials towards the bacteria surface. Our approach allows targeted antibiotic delivery to bacteria cell surface which allows the increase of the efficacy of the drug and also reduce off-target toxicity.

TB is a life threating infectious disease.[31] Pulmonary TB is caused mainly by *Mycobacterium tuberculosis* (*Mtb*) bacteria. Active TB is symptomatic while latent TB is asymptomatic and difficult to treat. In latent pulmonary TB, *Mtb* can lie dormant in lung tissue unaware to the immune system for years.[32] Immune system cannot eradicate the *Mtb* bacteria whilst it lies within cells of the lung tissue. Our nano-assembly is designed to target and kill these mycobacteria that survive within the lung epithelial cells. Previous nanotechnology-based drug delivery systems designed to target *Mtb* include recent work done by Tenland and coworkers.[33] Tenland et al. used mesoporous silica nanoparticles as a porous drug delivery nanocarrier loaded with antibacterial peptide NZX.[26,33] They demonstrated 88% reduction in *Mtb* from in-vivo studies. Ali and co-workers reported GNRs as delivery vehicles to deliver antibiotic rifampicin. GNRs also act as a source of inherent bactericidal activity against *Mtb*.[34] Li et al. reported combined antibiotic and PTT using core-shell up conversion nanoparticles carrying an anti-tuberculotic drug rifampin.[35] All these drug delivery systems, however, suffers from lack of targeting towards intracellular *Mtb*.

Our engineered nano-assembly apart from what was mentioned before have (a) colloidal stability

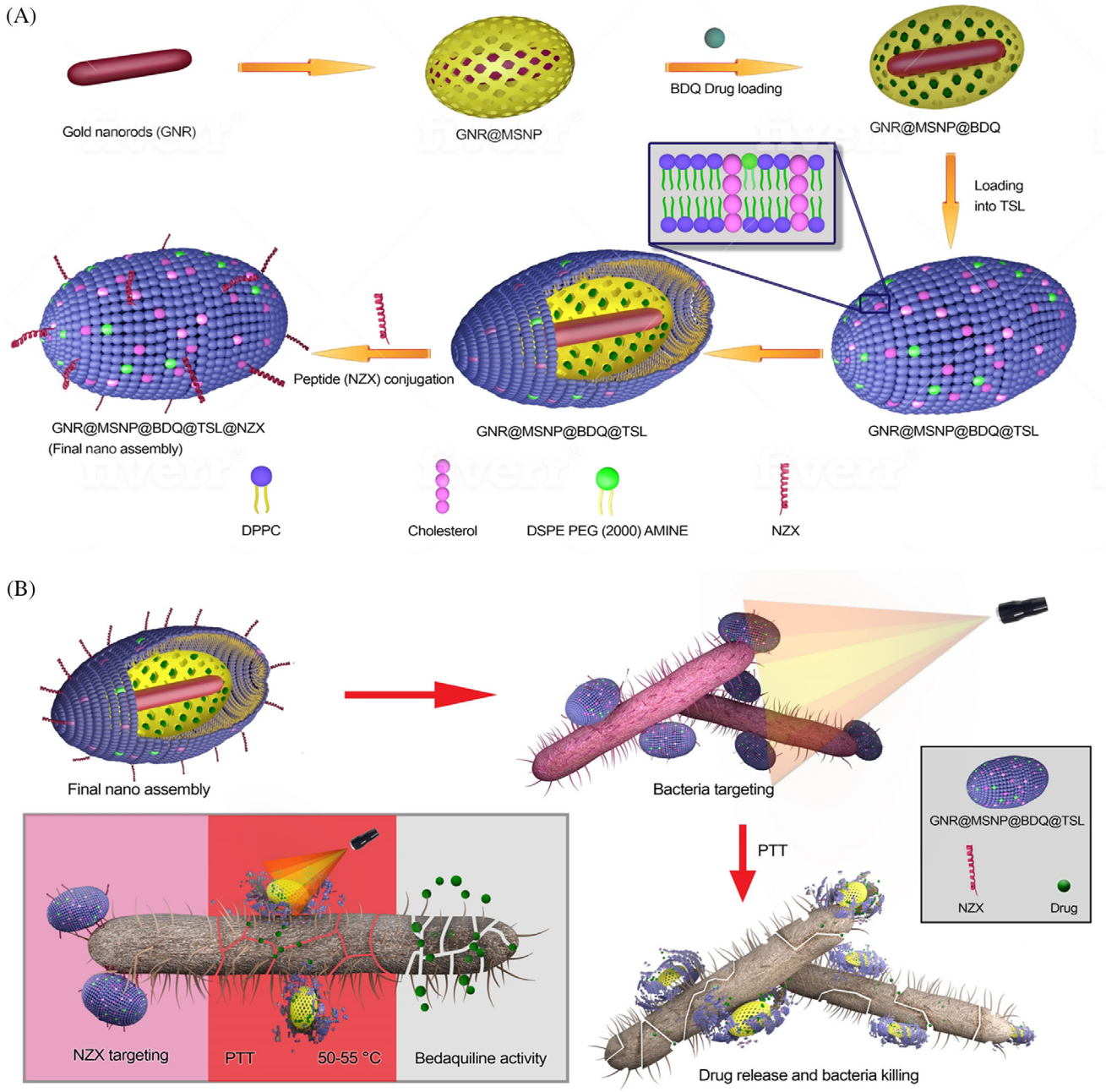

SCHEME 1 (A) Schematic illustration of stepwise synthesis of the final nano-assembly: (B) GNR@MSNP@BDQ@TSL@NZX. B, Application of final nano-assembly: GNR@MSNP@BDQ@TSL@NZX for targeting and killing *Msmeg* using 808 nm NIR laser light

(b) prevents premature drug release (c) increase internalization into infected host cells through TSL coating and NZX targeting peptide (d) control release of drug through melting of TSL. The antibacterial activity of the final nano-assembly GNR@MSNP@BDQ@TSL@NZX (Scheme 1), was observed against *Mycobacterium smegmatis* (*Msmeg*) in a series of in-vitro experiments. *Msmeg* is a biosafety level 1 (BSL-1) mimic of *Mtb*. We also assessed the ability of the nano-assembly to target and kill 99.9% *Msmeg* internalized within lung epithelial cells.

2 | RESULTS AND DISCUSSION

2.1 | Fabrication and characterization of nano-assembly

Fabrication of the final nano-assembly GNR@MSNP@BDQ@TSL@NZX was achieved in a stepwise manner as illustrated in Scheme 1A. GNRs were synthesized via seed method as described by El-Sayed et al., with some minor modifications.[36] As shown in the Figure 1A, the average length and width of GNRs

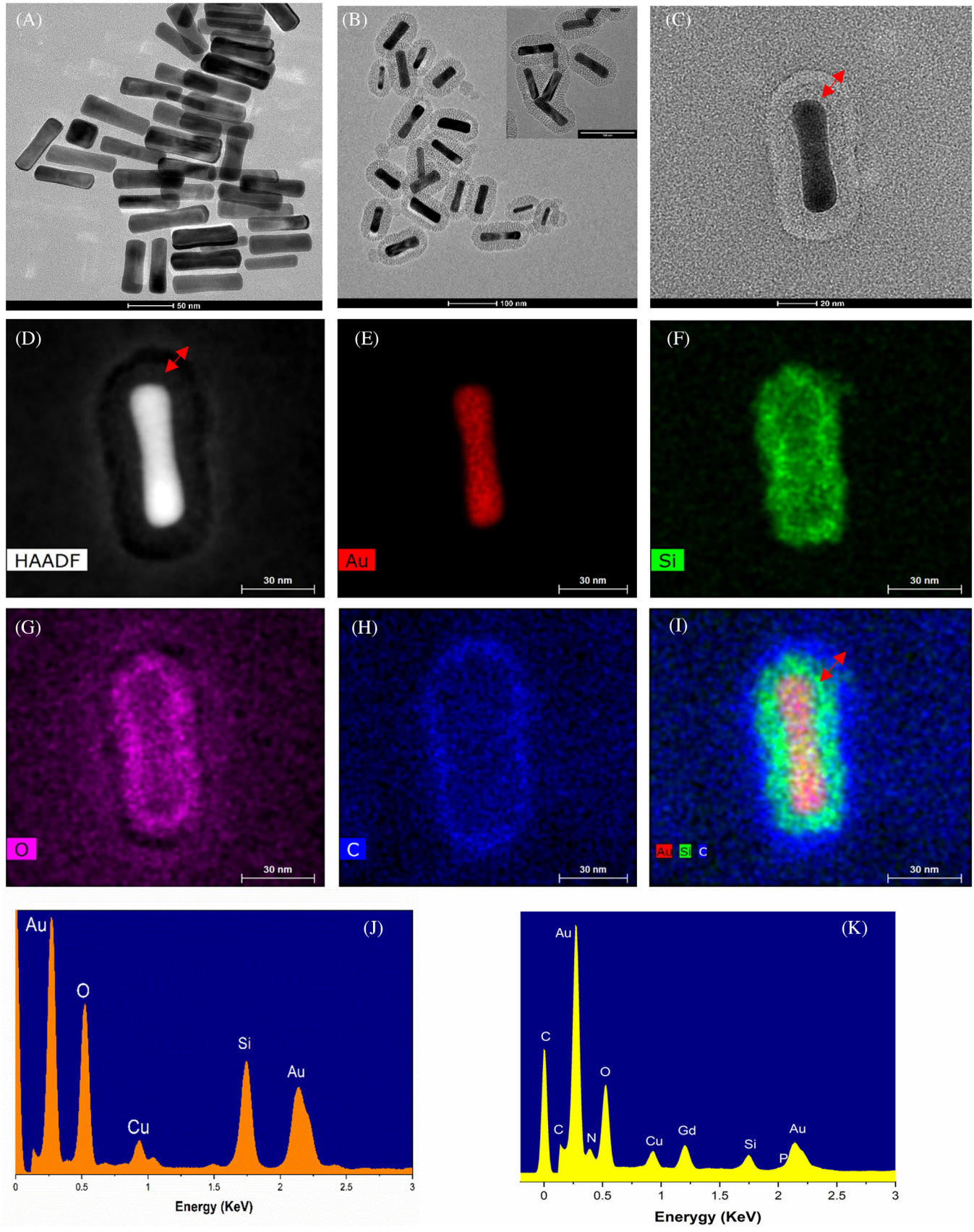

FIGURE 1 Characterization of nano-assemblies by TEM and STEM. (I) TEM images of (A) GNR (Scale bar = 50 nm), (B) GNR@MSNP (Scale bar = 100 nm) and (C) GNR@MSNP@BDQ@TSL (Scale bar = 20 nm). HAADF images of GNR@MSNP@BDQ@TSL which indicted presence of (E) gold, (F) silica, (G) oxygen, (H) carbon and (I) merged image (Scale bar = 30 nm). (J) EDS profile mapping of GNR@MSNP@BDQ and (K) GNR@MSNP@BDQ@TSL

were 42 ± 3.8 and 11.2 ± 1.1 nm and the calculated average aspect ratio was 3.8:1. GNRs displayed an uniform and well dispersed rod-like morphology (Figure 1A). GNRs coated with mesoporous silica shell were synthesized by modified protocol from Matsuura et al.[37] CTAB was used as a soft template, which creates the mesoporous silica shell structure during the polymerization of silane around the GNRs, to give GNR@MSNP.[38] TEM images (Figure 1B) show GNRs clearly encapsulated in a mesoporous silica shell (GNR@MSNP). The silica shell has an average thickness of 15 ± 3 nm and its porous structure can be clearly seen by TEM (Figure 1B). BDQ an anti-tuberculosis drug was encapsulated into the porous structure of the GNR@MSNP to create GNR@MSNP@BDQ. The GNR loaded mesoporous structure was wrapped by TSL to give GNR@MSNP@BDQ@TSL. The size of GNR@MSNP@BDQ@TSL were found to be 80 ± 3 nm (n = 20, n - number of nanoparticles) by TEM and the standard deviation was calculated by Image J software. The liposomal layer is visible through TEM as shown with red double headed arrow (Figure 1C). The shape of GNR@MSNP dictates the oblong shape of the TSL layer (Figure 1C). High-angle annular dark-field scanning transmission electron microscopy (HAADF-STEM) images (Figure 1E-I) show presence of the elements of gold (Au), silica (Si), oxygen (O) and carbon (C) present in the layers of GNR@MSNP@BDQ@TSL. The merged image in Figure 1I clearly show the individual layers overlaid on each other to show the final construct of GNR@MSNP@BDQ@TSL. HAADF images reveal the presence of carbons from the long hydrocarbons chains of lipids used to form the TSL. Which proves the presence of TSL surrounding GNR@MSNP@BDQ as indicated by red double headed arrow in the merged image of Figure 1I. The combined TEM (Figure 1C) and HAADF-STEM (Figure 1I) images clearly show TSL coating surrounding GNR@MSNP@BDQ.

The chemical composition of GNR@MSNPs and GNR@MSNP@TSL was analyzed by Energy dispersive X-ray spectroscopy (EDS). The EDS spectra of GNR@MSNPs (Figure 1J) clearly displayed the peaks of gold (Au), oxygen (O), and silica (Si). A peak for copper (Cu) was present in the EDS spectra (Figure 1J) because a Cu mesh TEM grid was used as a substrate. EDS spectrum of GNR@MSNP@BDQ@TSL (Figure 1K), shows the peaks for elements Au, Si, O and C. The presence of phospholipids in the TSL layer was indicated by the phosphorous (P) peak present in the EDS spectrum (Figure 1K). However, the peaks for P and Au overlap with one another (see Figure 1K). Therefore, to avoid confusion of using overlapping P peak to indicate the presence of TSL, we have used the presence of carbons (C) to indicate the presence of TSL layer. TSL is composed of lipids that have a long chain hydrocarbon for example DPPC lipid has a 40-carbon alkyl chain. HAADF-STEM image in Figure 1H shows the clear presence of C in the outermost TSL layer. The merged image in Figure 1I clearly shows the presence of C in the exterior of the nano-assembly.

The zeta potential was measured after addition of each layer to monitor the change in surface charge.[22] The altered surface zeta potential is shown in Figure 2A. The zeta potential of GNRs was 28 ± 0.59 mV, this is possibly due to the presence of positively charged CTAB on the surface. After silica coating the surface charge was reduced to -23.54 ± 0.8 mV due to the presence of abundant Si–OH groups. BDQ is hydrophobic and has high solubility in DMSO and little or no solubility in water. Therefore, zeta potential for BDQ was not obtained. After loading BDQ to MSNP, the zeta potential increased to +2.27 ± 0.76 mV. We hypothesize this is possibly due to the reduction in the available surface OH groups after loading of BDQ. TSL coating increased the zeta potential to +7.25 ± 0.6 mV owing to the presence of amine groups from DSPE-PEG 2000 amine on the surface. The cationic peptide NZX was conjugated to the to the abundant -NH_2 groups present on the surface of liposome through carbodiimide coupling chemistry. The cationic NZX is responsible for the final increase the zeta potential up to +11.6 ± 0.88 mV.

The UV-vis spectra clearly indicated two characteristic absorbance peaks for GNRs. The transverse surface plasmon resonance (TSPR) peak at 514 nm and longitudinal surface plasmon resonance (LSPR) peak at 790 nm. After the mesoporous silica coating the LSPR peak underwent a red shift towards 805 nm, this is due to the change in the local refractive index of the surrounding medium and changes in geometry. The laser was selected to match the new absorbance at 805 nm. There was no observable shift in the LSPR peak after the loading of BDQ drug and TSL wrapping (Figure 2B). The TSPR and LSPR peaks for all nano-assemblies are listed in table (Table S1).

The FT-IR spectra of the different components of the fabrication step are presented in Figure 2C. GNRs show -CH_2 symmetric and asymmetric vibrations at 2847 and 2870 cm^{-1}, respectively. The presence of a peak at 1473 cm^{-1} corresponds to the CH_2 scissoring modes of vibrations. In the fingerprint region, the bands at 960 and 817 cm^{-1} are consistent with C-O stretching and in plane C-H bending vibrations. The appearance of a peak at 1064 cm^{-1} (Si-O-Si stretching) the disappearance of symmetric (2847 cm^{-1}) and asymmetric (2870 cm^{-1}) vibrations which were seen for GNRs, proves the mesoporous silica coating on the surface of GNRs. After BDQ loading, the characteristic peaks appearing from benzene rings, C- H stretching: 2922 and 2914 cm^{-1} and C-C stretching: 1407 cm^{-1} were observed. The presence of N-H stretching at 1662 cm^{-1} and C-N stretching at 1230 cm^{-1} shows the presence of the primary amine group of BDQ which confirms the successful loading of BDQ to the nano-assembly. The symmetric

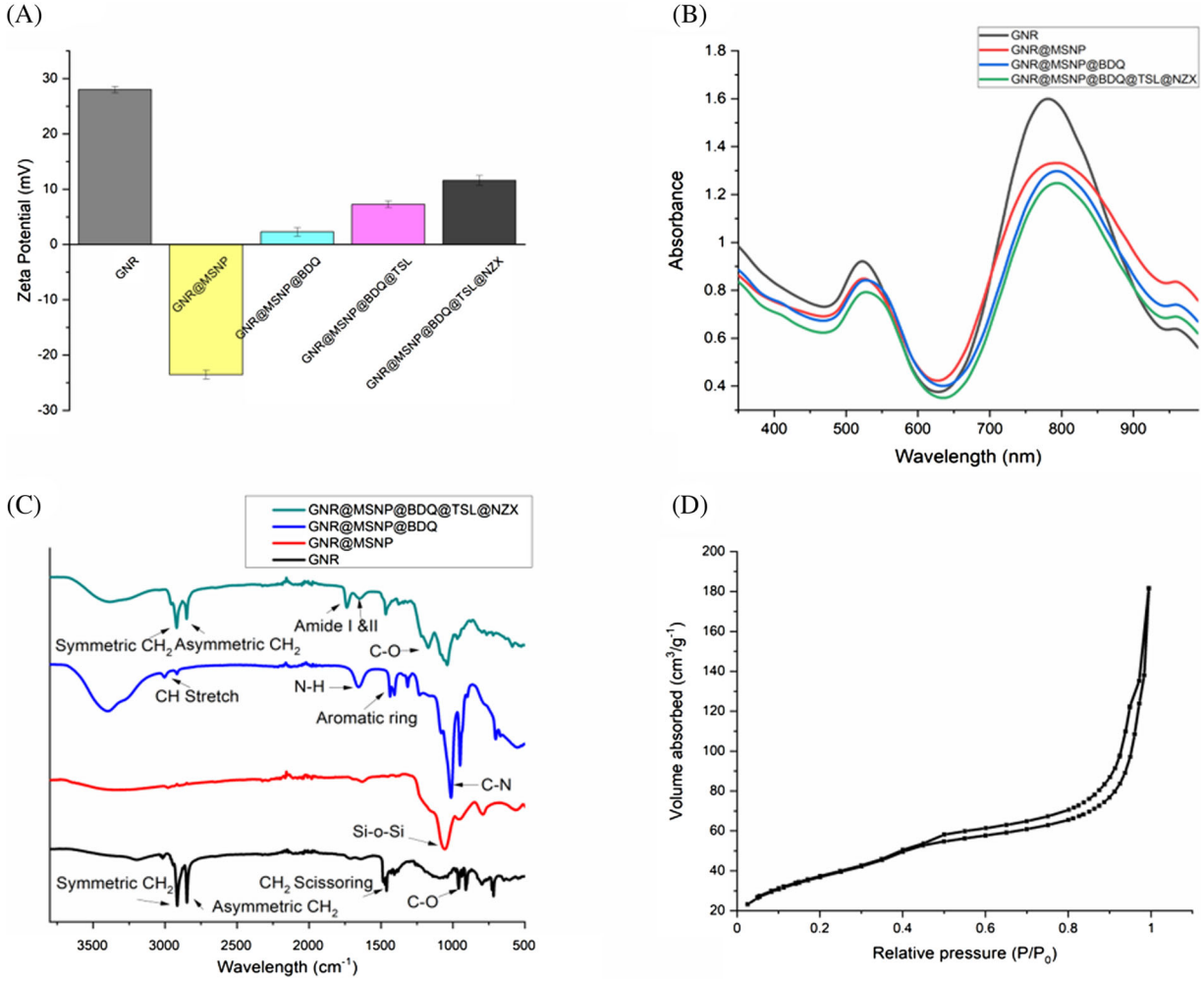

FIGURE 2 Characterization of nano-assemblies (A) zeta potential (B) UV-vis absorbance spectra (C) FT-IR spectra (D) N_2 adsorption−desorption isotherm of GNR@MSNP

and anti-symmetric -CH_2 stretching 2848 and 2918 cm^{-1} confirms the presence of the lipid layer on the surface of GNR@MSNP@BDQ. NZX was conjugated to the abundant -NH_2 groups present on the surface of TSL through EDC coupling chemistry. The -COOH groups of the peptide were activated with EDC and reacted with sulfo-NHS.[39] The sulfo-NHS of the peptide reacts with the –NH_2 groups on the TSL. The conjugation of NZX peptide on TSL introduces amide I and II bands at 1650 and 1540 cm^{-1}, and C-O stretching vibration at 1241 cm^{-1}. All characteristics peaks for various nano-assemblies are labelled in FT-IR spectra as well as listed in the Figure S3 and Table S2.

The N_2 adsorption–desorption isotherm and pore size distribution curves of GNR@MSNP are given in Figure 2D. This exhibits a typical type IV isotherm with a narrow pore size distribution with a mean of 19.13 ± 1.2 Å. This verifies mesoporous character of the MSNP shell. Through BET, the total surface area and pore volume of GNR@MSNP were quantified to be 53.852 m^2g^{-1} and 0.23 mL g^{-1}, respectively.

2.2 | Colloidal stability of nano-assemblies

The colloidal stability of GNR@MSNP and GNR@MSNP@TSL was monitored using UV-vis spectroscopy and DLS analysis. The localized surface plasmon resonance (LSPR) of gold nanoparticles (NPs) was affected by nanoparticle aggregation.[40] When plasmonic NPs aggregate individual plasmon oscillation can couple with each other through near-field interactions, resulting in coupled LSPR modes.[41] This impacts the distribution of the electric field around the nano-structure.[40,42] As a consequence, particle aggregation results in the broadening, reduction and red shift in the LSPR peak in the absorbance spectrum.[43] This was confirmed by a color shift of the colloid gold nanoparticles from deep red to purple, which is characteristic for an unstable plasmonic colloidal system.[44] The stability studies of GNR@MSNP and GNR@MSNP@TSL) were conducted at 37 °C in cell culture media for 5 days. As shown in Figure 3A, the LSPR

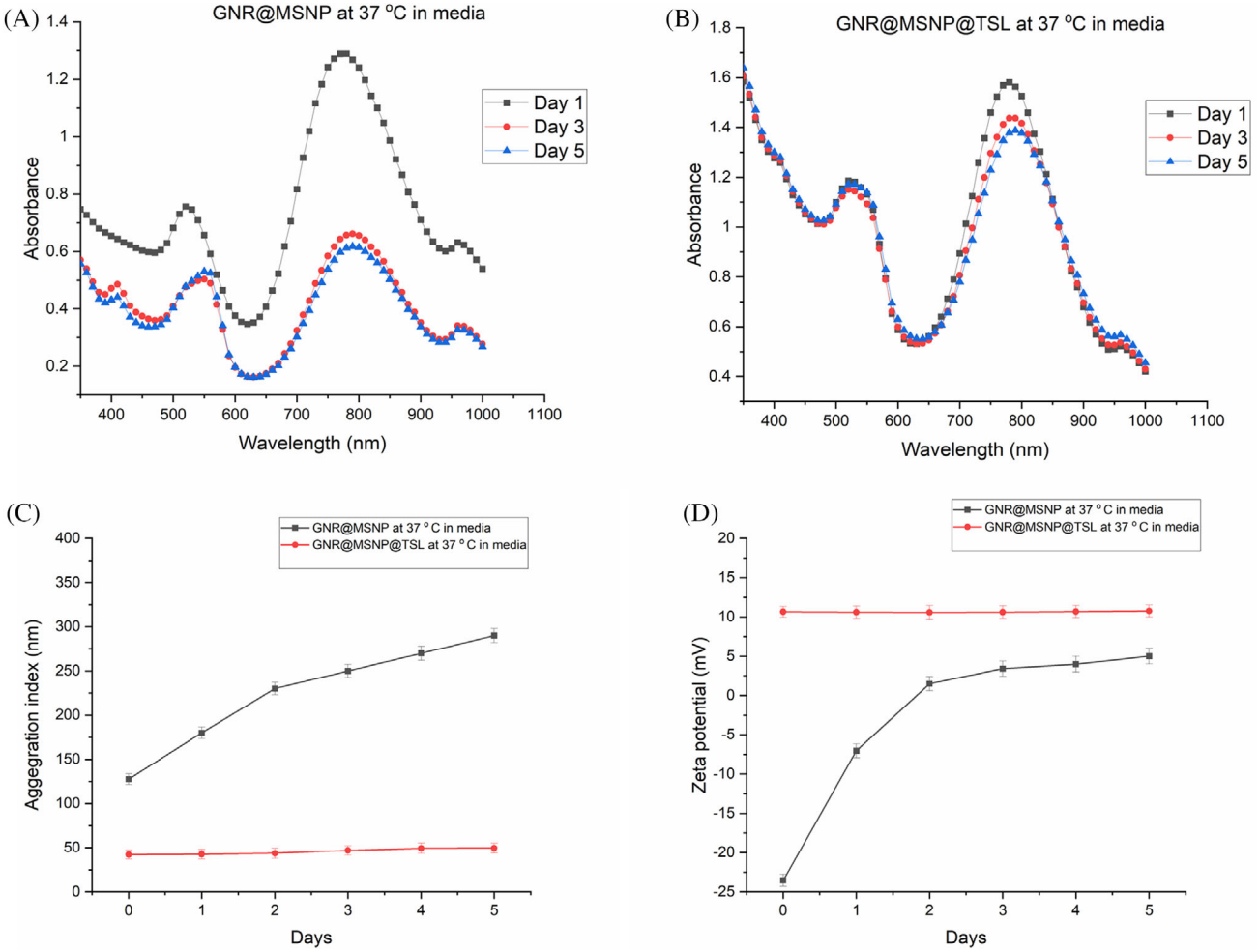

FIGURE 3 Colloidal stability analysis of GNR@MSNP and GNR@MSNP@TSL. UV-vis spectra of (A) GNR@MSNP (B) GNR@MSNP@TSL at 37 °C, in cell culture media (C) aggregation index (AI) of GNR@MSNP and GNR@MSNP@TSL (D) zeta potential of GNR@MSNP and GNR@MSNP@TSL in cell culture media at 37 °C

peak intensity for GNR@MSNP was reduced after day 1 when compared to GNR@MSNP@TSL. And therefore, GNR@MSNP was clearly not stable in media. However, with TSL coating (Figure 3B), GNR@MSNP@TSL was stable in cell culture media for 5 days.

Aggregation index (AI) was calculated for GNR@MSNP and GNR@MSNP@TSL and are shown in Figure 3C. The higher AI indicates, higher degree of aggregation, and represents lower colloidal system stability.[45,46] AI for GNR@MSNP was higher and increased with time in media at 37 °C. In GNR@MSNP@TSL, the AI values were low and constant with time in media at 37 °C. Therefore, GNR@MSNP@TSL shows better colloidal stability than GNR@MSNP.

Zeta potential was used to observe the stability of the nano-assemblies.[22] As shown in Figure 3D, zeta potential of GNR@MSNP changed from day 0 to 5 from -23.5 ± 0.7 up to +5.0 ± 0.9 mV. This continuous change in zeta potential in media suggests that GNR@MSNP was unstable. In contrast, GNR@MSNP@TSL, displayed a constant zeta potential value +10.6 ± 0.7 mV up to 5 days. These observations also reveal the stability of GNR@MSNP@TSL. The LSPR peak intensity, AI and zeta potential all indicate GNR@MSNP@TSL has more colloidal stability than GNR@MSNP. Photographic evidence of the comparative stability of GNR@MSNP@TSL and GNR@MSNP is shown in Figure S4. All the above stability parameters indicate that the TSL coating improves the colloidal stability of the nano-assembly; therefore, promoting their suitability for antibacterial applications both in vitro and in vivo.

2.3 | Photothermal effect of GNRs and NIR laser activated drug release

The photo/thermo responsive properties of nano-assembly were evaluated via a series of experiments. A 808 nm laser diode was selected to match the

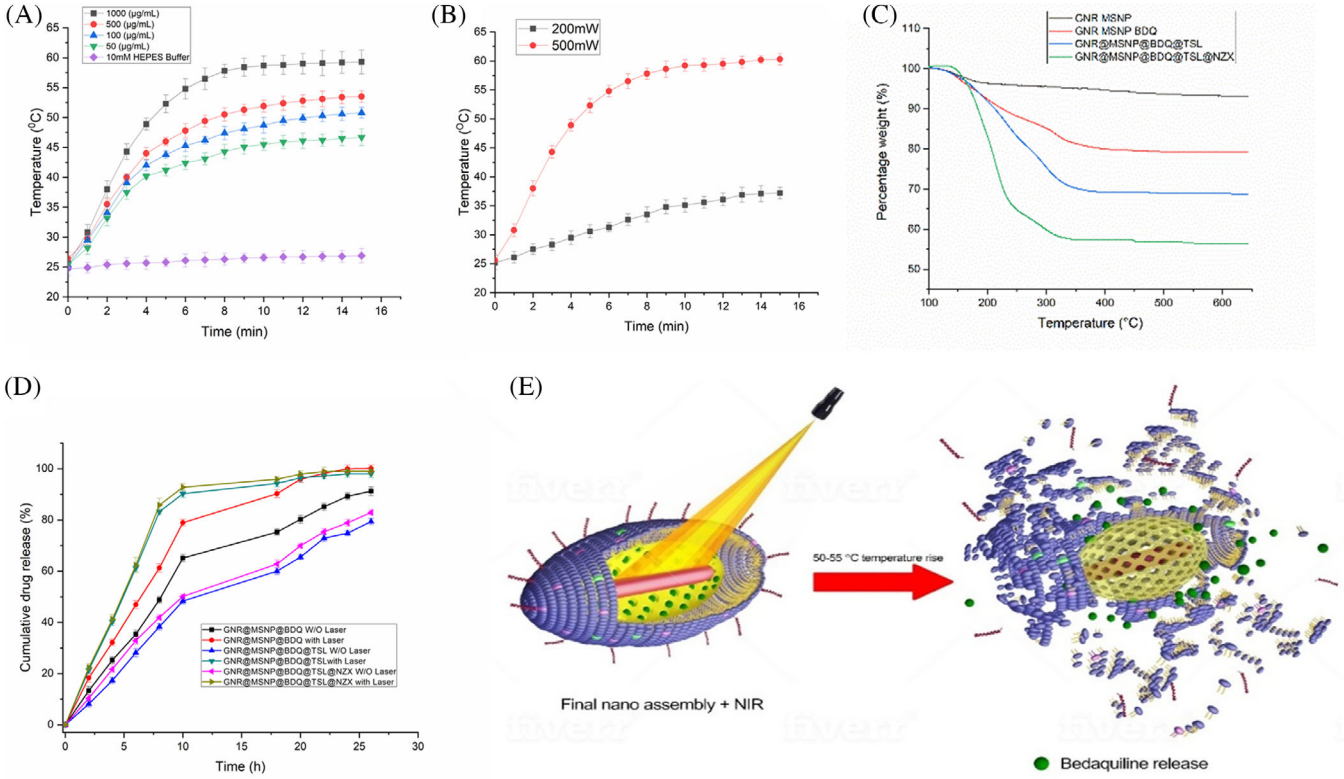

FIGURE 4 NIR triggered drug release and photothermal properties of nano-assemblies (A) Photothermal effect of final nano-assembly GNR@MSNP@BDQ@TSL@NZX at different concentrations using a 808 nm, 500 mW, laser for 15 minutes. (B) The temperature profile of GNR@MSNP@BDQ@TSL@NZX (1 mg mL^{-1}) with different laser power intensities (C) TGA analysis of various nano-assemblies. (D) Cumulative drug release profile of BDQ from various nano-assemblies with and without laser irradiation (808 nm, 500 mW, 15 minutes). (E) Schematic representation of NIR triggered degradation of the liposome followed by the release of BDQ from the final nano-assembly.

LSPR peak associated with the final nano-assembly GNR@MSNP@BDQ@TSL@NZX. The photothermal efficiencies of the final nano-assemblies were evaluated in-vitro, after irradiation with 808 nm laser at 500 mW for 15 minutes. A 25 mm objective lens was used to tightly focus the laser light onto the sample (spot size ~2 mm, diameter). Figure 4A shows the photothermal capacity of the final nano-assembly GNR@MSNP@BDQ@TSL@NZX at different concentrations. Under these conditions, the temperature of the final nano-assembly GNR@MSNP@BDQ@TSL@NZX increased to 58 ± 3.0 °C at its highest concentration (1000 µg mL^{-1}) and 45 ± 2.0 °C for the lowest concentration (50 µg mL^{-1}). The control containing 10 mM HEPES solution increased by only 2 °C, indicating that the elevation of temperature was caused primarily by the PT effect of GNRs. The temperature increase of the final nano-assembly GNR@MSNP@BDQ@TSL@NZX, was positively correlated to the concentration, laser power intensity and irradiation time (Figure 4A,B). Encapsulation efficiency and drug loading efficiency of BDQ were analyzed to be, respectively, 65.0 ± 0.5% and 14.6 ± 0.9% by HPLC. The quantitative analysis of nano-assemblies after each step of synthesis was done through TGA.[22] The results are shown in Figure 4C and Table S3. Percentage (%) weight loss between the GNR@MSNP@BDQ and GNR@MSNP was calculated to determine the amount of BDQ loaded onto GNR@MSNP. The BDQ loading was found to be 16 ± 0.5% in GNR@MSNP. Additionally, the percentage weight loss between GNR@MSNP@BDQ@TSL and GNR@MSNP@BDQ displayed that the coated lipid layer was 10 ± 1.6% of GNR@MSNP@BDQ@TSL. Finally, NZX loading on GNR@MSNP@BDQ@TSL was quantified by TGA analysis between the GNR@MSNP@BDQ@TSL@NZX and GNR@MSNP@BDQ@TSL. The total peptide NZX loading was found to be 12 ± 1.5% on GNR@MSNP@BDQ@TSL.

NIR-triggered drug release of the final nano-assembly GNR@MSNP@BDQ@TSL@NZX was performed in 0.5% w/w SLS in 10 mM HEPES buffer with and without NIR laser irradiation. As shown in Figure 4D GNR@MSNP@BDQ without laser irradiation cumulatively released 65.1 ± 1.4% of BDQ within 10 hours. With laser irradiation GNR@MSNP@BDQ cumulatively released 78.9 ± 1.8% in the same span of 10 hours. This clearly indicates that the subsequent temperature

increase with laser irradiation has increased the non-specific release of BDQ. GNR@MSNP@BDQ@TSL demonstrated only a 48.32 ± 1.5% BDQ release in a similar time frame, without laser irradiation. The presence of TSL therfore has clearly helped to reduce non-specific release of encapsulated BDQ when compared to that of GNR@MSNP@BDQ under similar conditions. GNR@MSNP@BDQ@TSL released 90.2 ± 1.4% of BDQ within 10 hours after laser irradiation. Final nano-assembly GNR@MSNP@BDQ@TSL@NZX demonstrated a similar behavior with 92.7 ± 1.5% of BDQ release upon laser irradiation and only 50.1 ± 0.9% of BDQ was released in absence of laser (Figure 4D). It is apparent from the above results that TSL plays a role in reducing premature BDQ release. Laser-irradiation generates localized heat from GNR, which subsequently weakens the interactions between the mesoporous silica matrix and enhanced the permeability of the TSL (Figure 4E). TSL is composed of a thermo-sensitive phosphocholine lipid (DPCC 85% molar ratio), and the melting of DPCC increases the permeability of TSL.[47] The drug, BDQ, release profile upon laser irradiation, suggest that the melting of the TSL resulted in the release of the drug from final nano-assemblies (Figure 4D). The melting of TSL (48 ± 3 °C) was further evaluated by calcein dye release assay. The calcein dye release with respect to laser irradiation time and with increase in temperature is shown in supplementary information (Figure S5).

2.4 | Antimicrobial activity of nano-assemblies

The in-vitro antimicrobial activity of the nano-assemblies against *Msmeg* was determined using WST-8, a colorimetric bacterial viability assay, and bacterial colony counting assay. WST-8 produces a yellow color formazan dye upon the reduction of tetrazolium by dehydrogenase enzymes in live bacteria.[48] The absorbance of produced formazan was measured at 460 nm, which is proportional to the number of live bacteria.[48] The MIC was reported with respect to the encapsulated BDQ in the nano-assemblies at their MIC concentrations. The MIC established by colorimetric assay and verified by colony counting, was found to be 40 ng mL^{-1} for the free drug BDQ. The MIC of final nano-assembly GNR@MSNP@BDQ@TSL@NZX (with laser) was 2 ng mL^{-1} with respect to the encapsulated BDQ (Table 1). This shows that BDQ encapsulated in final nano-assembly is 20-fold efficacious than the free drug BDQ. The higher efficacy is due to the combitherapy of PTT working together with antibiotic.

The quantitative antibacterial efficacy of nano-assemblies was further analyzed using colony counts and expressed as a percentage of viable bacteria (Figure 5A). The antibacterial activity of the nano-assemblies was compared to one-another using percentage of viable bacteria present after treatment with various nano-assemblies with (+) and without (−) laser (Figure 5A). The percentage viable bacterial cell obtained from bacterial colony counts from agar plates is shown in the photographs of Figure 5B. *Msmeg* exposed to GNR@MSNP@BDQ@TSL@NZX (+ laser) exhibited 5 ± 1.2% bacterial viability and GNR@MSNP@BDQ@TSL@NZX (− laser) had 78 ± 1.9% bacterial viability. Therefore, it is clear that laser irradiation is vital to the antibacterial activity of the final nano-assembly. *Msmeg* exposed to GNR@MSNP@BDQ + laser and − laser exhibited 33 ± 2.1% and 68 ± 1.5% bacterial viability, respectively. Because the lack of TSL, GNR@MSNP@BDQ + laser exposure cause high release of BDQ.

TABLE 1 MIC of materials. MIC is reported with respect to the encapsulated BDQ in the nano-assemblies*

Materials	MIC [ng mL^{-1}]
NZX	400 ± 1.8
BDQ	40 ± 1.5
GNR@MSNP@BDQ	25 ± 1.8*
GNR@MSNP@BDQ + Laser	10 ± 1.5*
GNR@MSNP@BDQ@TSL@NZX	30 ± 1.9*
GNR@MSNP@BDQ@TSL@NZX + Laser	2 ± 0.8*

In both occasions where *Msmeg* was treated + laser and GNR@MSNP - laser, had similar bacterial viability (98 ± 1.7), therefore little or no antibacterial activity was seen with GNR@MSNP. However, when *Msmeg* was treated with GNR@MSNP + laser the viability reduced to 78.5 ± 2.5. The heat produced by GNRs upon laser irradiation cause the viability of bacteria to decrease. Photographs of selected bacterial plates after treatment with nano-assemblies can be seen in Figure 5B, and they are relatable to the MIC results. Figure 5C shows a hypothetical illustration of GNR@MSNP@BDQ@TSL@NZX that effectively target and kill bacteria upon laser irradiation.

It has been established previously that ROS can be produced by bacteria in response to heat stress during PT treatment.[49,50] Therefore, establishing the presence of ROS and quantification of ROS is useful when the antibacterial efficacy of the material is related to PT activity.[50] ROS produced was measured quantitatively by a fluorescent ROS assay and fluorescence produced was imaged through fluorescence microscopy (Figure 6). *Msmeg* + laser displayed slight green fluorescence (Figure 6A-B) suggesting that *Msmeg* produces a small quantity of ROS when exposed to laser. In contrast, comparatively larger amount of ROS was generated when *Msmeg* was

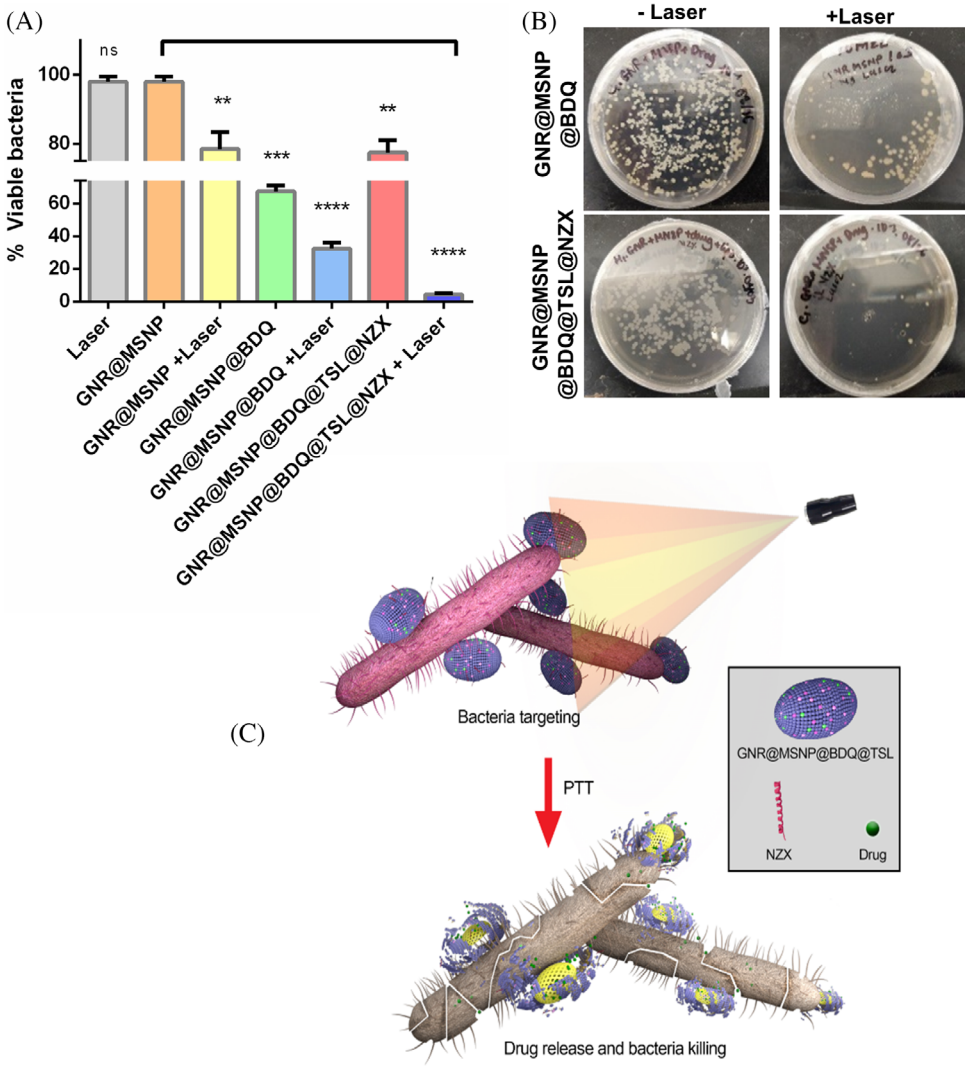

FIGURE 5 In-vitro antibacterial and PT activity. (A) Percentage of viable bacteria after treatment with the nano-assemblies ± laser irradiation. (B) Photographs displayed effect of laser on nano-assemblies after treating with *Msmeg* by colony count. (C) Schematic illustration of how final nano-assembly GNR@MSNP@BDQ@TSL@NZX targets and kills bacteria (grey color bacteria-dead bacteria) upon laser irradiation. The data were presented as the mean ± SD (n = 3). ns (non-significant), $^{**}P < 0.01$, $^{***}P < 0.001$, and $^{****}P < 0.0001$. A, $^{****}P < 0.0001$ indicated the data to be more significant when compared to $^{***}P < 0.01$ and $^{**}P < 0.01$ by One-way ANOVA

treated with GNR@MSNP@BDQ + laser (Figure 6A-D). *Msmeg* treated with GNR@MSNP@BDQ@TSL@NZX + laser displayed further green fluorescence (Figure 6A-F) indicative of higher ROS production. Quantitative analysis of ROS production, measured as fluorescence intensity, is shown in Figure 6B. These results are consistent with the fluorescent images (Figure 6B).

Live/dead assay was also done to complement the other antibacterial assays. In the live/dead assay SYTO9 and PI fluorescent stains were used to stain intact and damaged bacterial cells (Figure 7). SYTO 9 green, fluorescent dye penetrates the cell membrane of both live and dead bacterial cells while PI red fluorescent dye penetrates bacterial cells with damaged membranes.[51]

In the presence of both stains, bacteria with intact cell membranes appear fluorescent green, whereas cell membrane-compromised bacteria appear in red fluorescent. BDQ, GNR@MSNP@BDQ + laser and GNR@MSNP@BDQ@TSL@NZX + laser was incubated with *Msmeg* followed by stained with SYTO9/PI and results were observed through fluorescence microscopy. *Msmeg* treated with BDQ showed more green and less red fluorescence indicating the presence of more live bacteria as compared to dead bacteria (Figure 7A). The GNR@MSNP@BDQ + laser displayed an increase in red fluorescent intensity which suggests that some bacteria cells had compromised cell membranes (Figure 7B). *Msmeg* treated with final nano-assembly

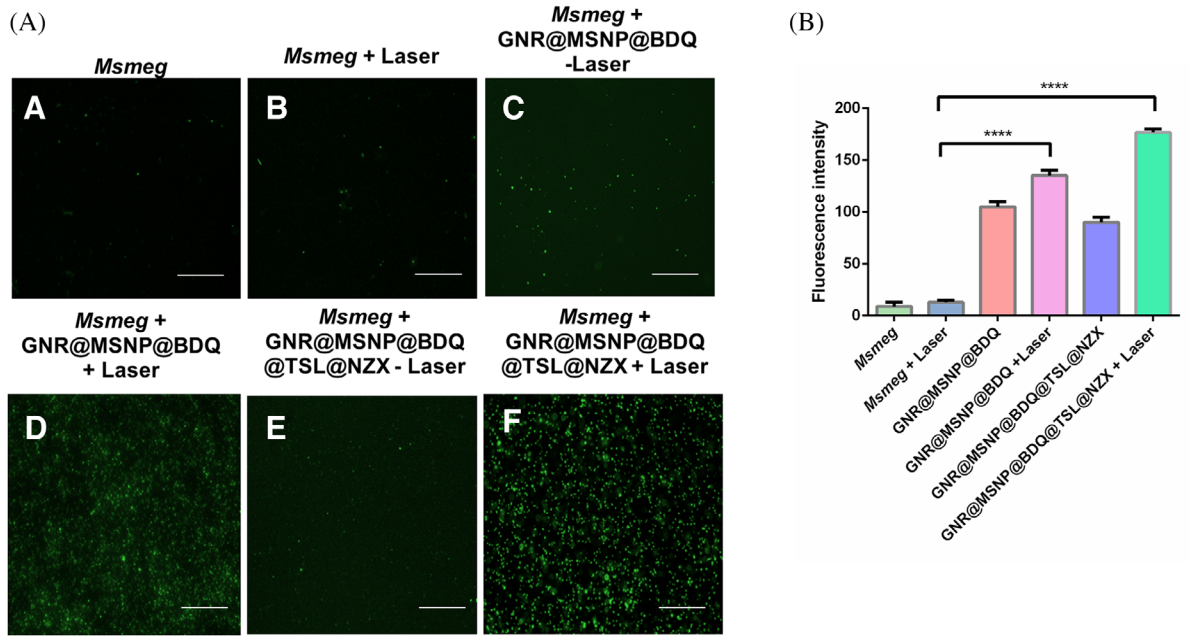

FIGURE 6 Reactive oxygen species (ROS) determined after treating *Msmeg* with nano- assemblies. Induced ROS is indicated by green fluorescence (A-A) *Msmeg* + without laser exposure, (A-B) *Msmeg* + with laser, (A-C) *Msmeg* + GNR@MSNP@BDQ + without laser, (A-D) *Msmeg* + GNR@MSNP@BDQ + with laser, (A-E) *Msmeg* + GNR@MSNP@BDQ@TSL@NZX + without laser, (A-F) *Msmeg* + GNR@MSNP@BDQ@TSL@NZX + with laser. Scale bars represent 1 μm. (B) Quantitative determination of ROS generation detected by fluorometric intracellular ROS assay. A, ****$P < 0.001$ indicates that data is statistically significant by one-way ANOVA

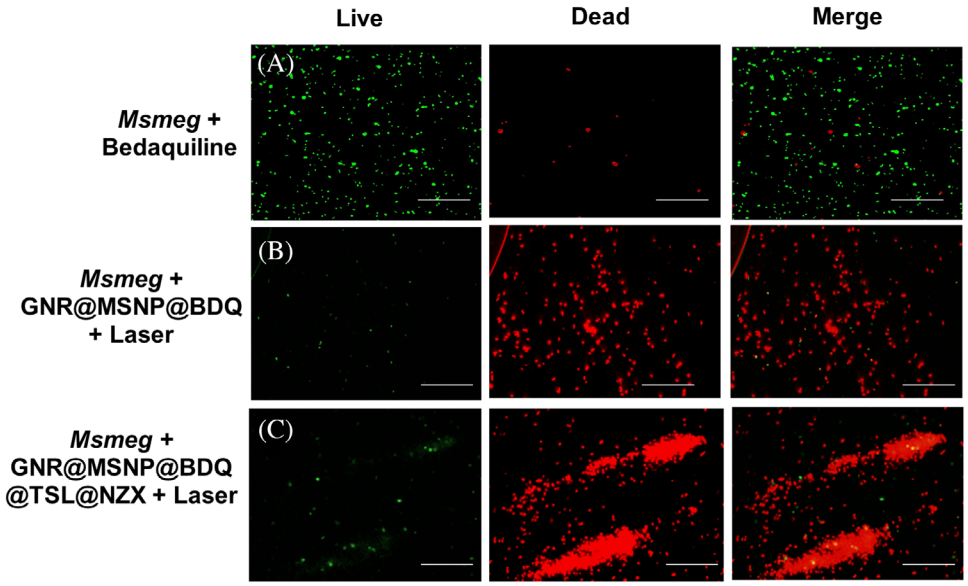

FIGURE 7 Fluorescence microscopy images of the live/dead assay. Fluorescence microscopy images showing the presence of live bacteria (green) and dead bacteria (red) following treatment of *Msmeg* with (A) BDQ (B) GNR@MSNP@BDQ + laser, and (C) GNR@MSNP@BDQ@TSL@NZX + laser (scale bars represent 50 μm)

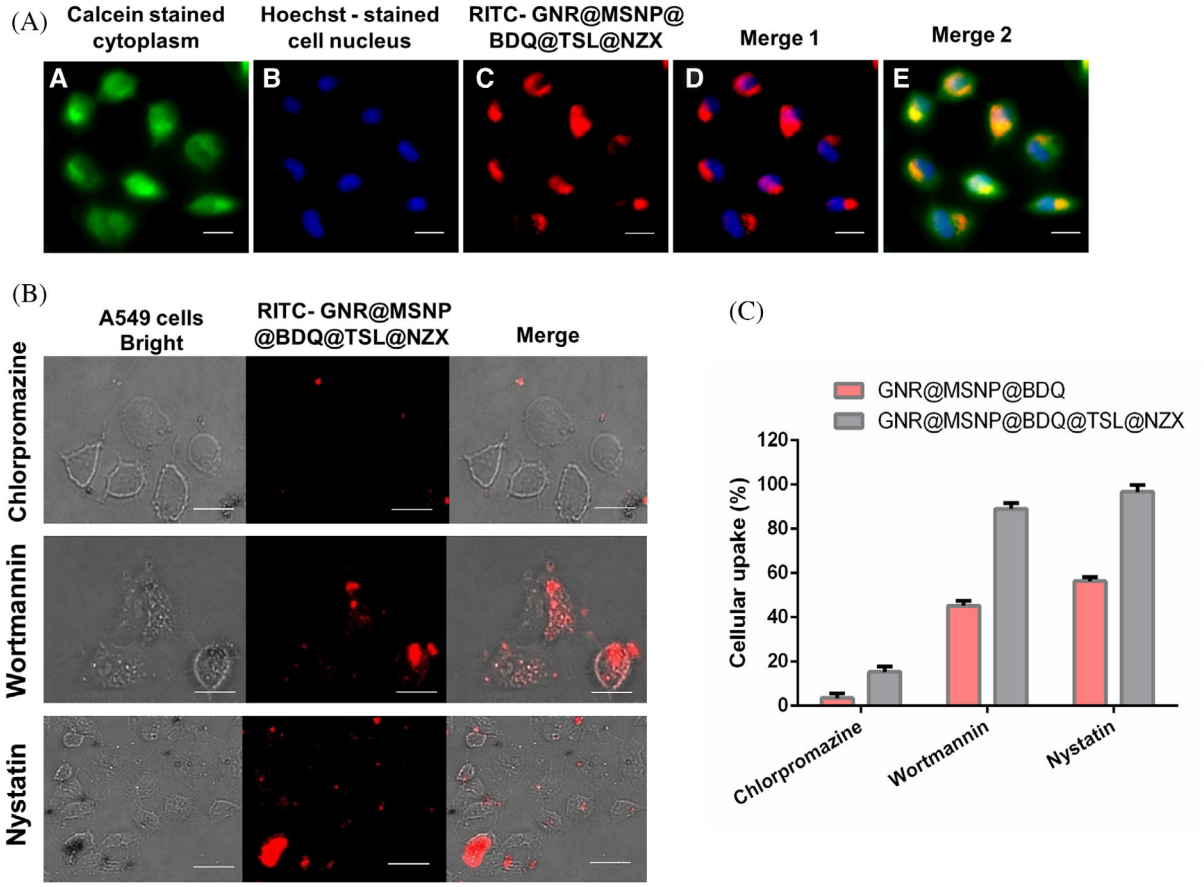

FIGURE 8 Selective cellular uptake of GNR@MSNP@BDQ@TSL@NZX by A549 cells. (A) Intracellular uptake of the final nano-assembly GNR@MSNP@BDQ@TSL@NZX by A549 cells. A549 cells are stained with calcein dye (green), cell nucleus stained with Hoechst dye (blue), nano-assemblies were labelled with red fluorescent RITC dye (red). Scale bar: 10 μm. (B) Evaluation of cell uptake mechanism of nano-assemblies by A549 cells under different endocytosis inhibitory conditions - fluorescence microscopy - A549 cells shown in bright field and nano-assemblies were tagged with RITC (Scale bar = 10 μm). (C) Shows quantitative intracellular uptake of GNR@MSNP@BDQ and GNR@MSNP@BDQ@TSL@NZX by A549 cells after inhibitor treatment

GNR@MSNP@BDQ@TSL@NZX + laser had high bacterial aggregation with high amount of red fluorescence, compared to free BDQ and GNR@MSNP@BDQ + laser. Aggregation can also be related to NZX mediated targeting and subsequent cross linking of bacteria (Figure 7C).

2.5 | Assessing intracellular antibacterial activity of nano-assemblies

Intracellular uptake of the nano-assemblies by A549 lung cells was visualized by fluorescent microscopy. As shown in Figure 8A cytoplasm of lung cells was stained with calcein a green, fluorescent dye (Figure 8A-A). Nucleus stained with Hoechst blue, fluorescent dye (Figure 8A-B) and nano-assemblies with RITC red fluorescent dye (Figure 8A-C). Figure 8A-D shows red fluorescent nano-assemblies were distributed in the lung cell close to the nucleus. Figure 8A-E clearly shows yellow/orange color which occur from the green color of calcein merging with the red fluorescence from the cytoplasm. Which proves GNR@MSNP@BDQ@TSL@NZX was effectively taken up by the A549 cells and distributed throughout the cells after 3 hours of incubation.

The mechanism for internalization of nano-assemblies into the lung cells were monitored by fluorescence microscopy (Figure 8B). The cellular uptake mechanism of RITC labelled GNR@MSNP@BDQ and GNR@MSNP@BDQ@TSL@NZX in lung cells were determined under different endocytosis inhibited conditions. Specific endocytosis inhibitors: chlorpromazine - inhibitor of clathrin-mediated endocytosis, nystatin—inhibitor for caveolin- dependent endocytosis and wortmannin-macropinocytosis inhibitor were investigated to study the mechanism of cellular uptake.[52] We have also quantified the cellular uptake of nano-assemblies using fluorescent assays. The fluorescence microscopy images reveal little or no visible red fluorescent

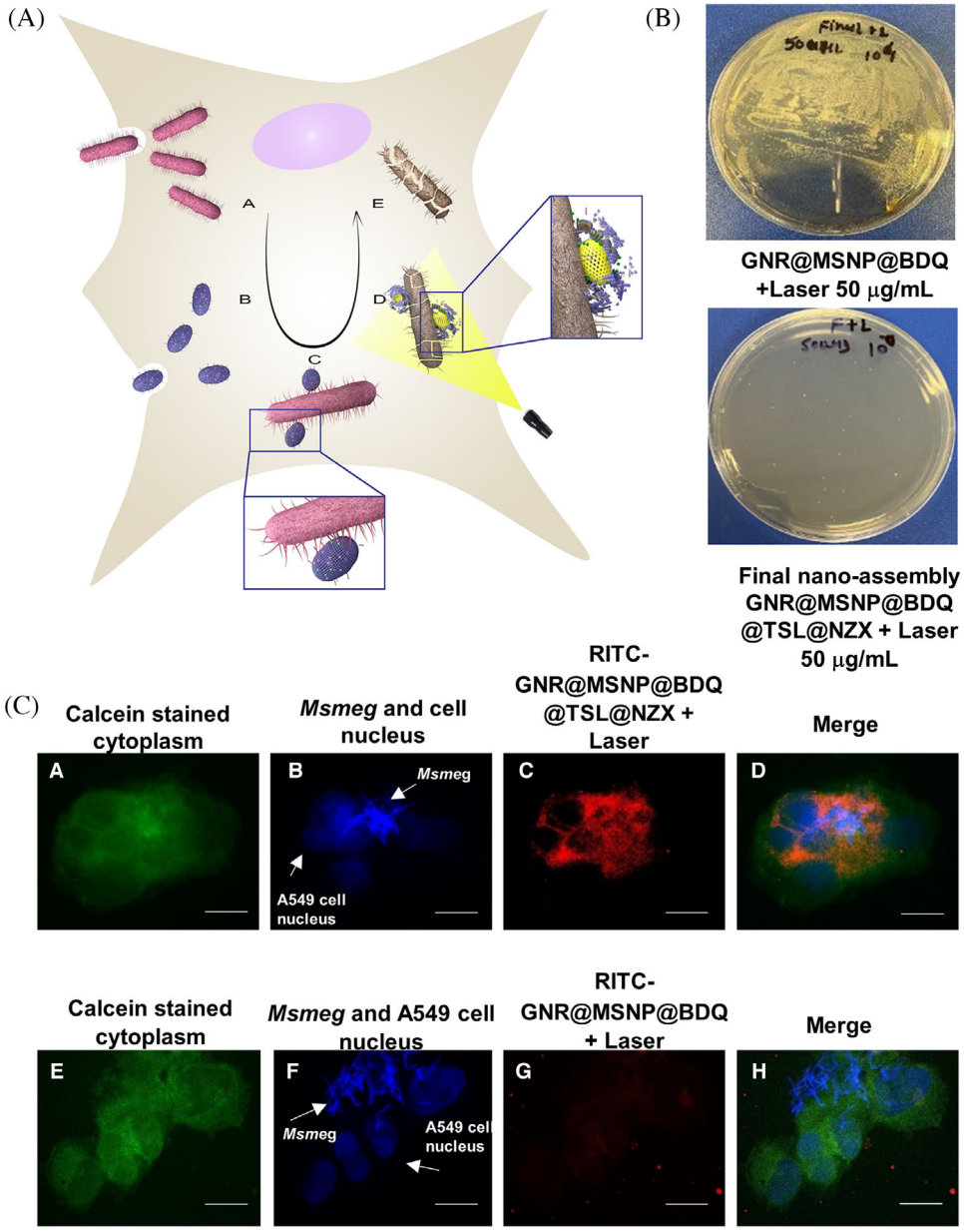

FIGURE 9 Intracellular antibacterial activities in *Msmeg* infected A549 cells. (A) Schematic illustration of the bacterial infection and treatment studies with A549 cells: A- infection of A549 cell with *Msmeg*, B- treatment with nano-assemblies C-NZX mediated adhesion of GNR@MSNP@BDQ@TSL@NZX to *Msmeg*, D- disintegration of TSL and BDQ release after NIR laser exposure, E- complete degradation of *Msmeg*. (B) Photographs of agar plates, of cultured intracellular *Msmeg* remaining after treatment with GNR@MSNP@BDQ and GNR@MSNP@BDQ@TSL@NZX. (C) Intracellular bacteria targeting capacity of nano-assemblies by A549 cells analyzed through fluorescent microscopy. A549 cells are stained with calcein dye (green), *Msmeg* bacteria and A549 cell nucleus stained with Hoechst dye (blue), nano-assemblies were labeled with red fluorescent RITC dye (red). Scale bars represent 5 μm

GNR@MSNP@BDQ@TSL@NZX in chlorpromazine treated lung cells (Figure 8B). Which indicates chlorpromazine treated lung cells have inhibited uptake of GNR@MSNP@BDQ@TSL@NZX. However, uptake of GNR@MSNP@BDQ@TSL@NZX into lung cells was not hindered when treated with wortmannin and nystatin (Figure 8B). These observations suggested that nano-assemblies trafficking occurred preferably through a clathrin-mediated endocytosis.

To investigate the role of TSL in cellular uptake, we quantified the cellular uptake of nano-assemblies GNR@MSNP@BDQ@TSL@NZX and GNR@MSNP@BDQ by measuring intracellular fluorescent intensity using fluorescent microplate reader. As shown in Figure 8C,

chlorpromazine—inhibitor of clathrin-mediated endocytosis, significantly inhibited both GNR@MSNP@BDQ and GNR@MSNP@BDQ@TSL@NZX delivery into lung cells. The quantified intracellular uptake of GNR@MSNP@BDQ and GNR@MSNP@BDQ@TSL@NZX was 3.5 ± 1.2% and 15.34 ± 2.5%, respectively. Even in the presence of inhibitor, higher amount of GNR@MSNP@BDQ@TSL@NZX uptake was found in lung cells. Which points out that the inclusion of TSL and NZX increases the ability to internalize. Throughout all inhibitory assays GNR@MSNP@BDQ has consistently shown lesser amount of uptake (Figure 8C).

These studies collectively suggested that the nano-assemblies mediated drug delivery occurred preferably through a clathrin-mediated endocytosis and nano-assemblies internalization enhanced due to having liposome and NZX cationic peptide. Liposome coating is known to enhance cellular uptake of nano-assemblies due to interaction with lipophilic cell membrane that allows cellular entry of nanoparticles by various endocytosis pathways.[52] In addition to that, TSL was modified with cationic peptide NZX, so due to electrostatic interaction with negatively charged cell membrane, the cellular uptake was higher for GNR@MSNP@BDQ@TSL@NZX.

The antibacterial activity of GNR@MSNP@BDQ@TSL@NZX within lung cells was assessed by quantifying their ability to target and kill intracellular *Msmeg* bacteria. Schematic illustration of *Msmeg* infection studies with A549 cells is shown in Figure 9A. A549 lung cell were infected with a concentration of 17×10^4 CFU mL^{-1} *Msmeg*. From the starting concentration, 8×10^4 CFU mL^{-1} of *Msmeg* was internalized into the lung cells. *Msmeg* internalized into lung cells were quantified using bacterial colony count. The *Msmeg* infected lung cells were treated with 50 μg mL^{-1} concentration of GNR@MSNP@BDQ and the GNR@MSNP@BDQ@TSL@NZX in the presence of laser. After treating with nano-assemblies, lung cells were lysed and lysates were plated on agar plates.

Lung cells treated with GNR@MSNP@BDQ@TSL@NZX + laser, had 22 CFU mL^{-1} of intracellular *Msmeg* after treatment (Figure 9B). This is a significant decrease of 99.9% of intracellular *Msmeg*. In contrast, treatment with GNR@MSNP@BDQ + laser, reduced intracellular *Msmeg* only up to 3×10^4 CFU mL^{-1} (Figure 9B), which is a 37.5% reduction in intracellular *Msmeg*. These results clearly demonstrate targeting ability and high antibacterial efficacy of the laser irradiated GNR@MSNP@BDQ@TSL@NZX which inhibits 99.9% intracellular *Msmeg* (Figure 9B).

The ability of nano-assemblies to target *Msmeg* within lung cells was also evaluated by confocal fluorescence microscopy. For confocal fluorescence microscopy, A549 cell cytoplasm was stained with calcein green, *Msmeg* and A549 cell nucleus stained with Hoechst blue. GNR@MSNP@BDQ@TSL@NZX and GNR@MSNP@BDQ were conjugated with RITC—red fluorescent dye. Fluorescent merge image (Figure 9C-D) clearly shows that GNR@MSNP@BDQ@TSL@NZX surrounding the intracellular *Msmeg* bacteria resident in lung cells. While little or no GNR@MSNP@BDQ are seen within lung cells infected with *Msmeg* (Figure 9C-H). These results agree with TEM analysis where morphological changes on bacteria was observed upon treated with laser irradiated nano-assemblies (Figure S6). Furthermore MTT, a mammalian cell viability assay was conducted to evaluate any cytotoxic effect of laser and nano-assemblies treatment on lung cells. Lung cells were treated with GNR@MSNP, GNR@MSNP@BDQ and GNR@MSNP@BDQ@TSL@NZX with laser irradiation. As shown in Figure 10, A549 lung cells did not show significant cytotoxicity and lung cell viability was close to 100%. Live-dead assay was also performed to evaluate cytotoxicity towards lung cells. The methods and results are explained in Figure S7. It is apparent through both the MTT assay and live-dead assay, laser irradiated treatment has minimal cytotoxic effects on the lung cells.

The overall results indicate that the final nano-assembly GNR@MSNP@BDQ@TSL@NZX with laser treatment serves as an effective drug delivery platform that combines the antimicrobial efficacy of the antibiotic with PTT to target and inhibit even intracellular mycobacteria.

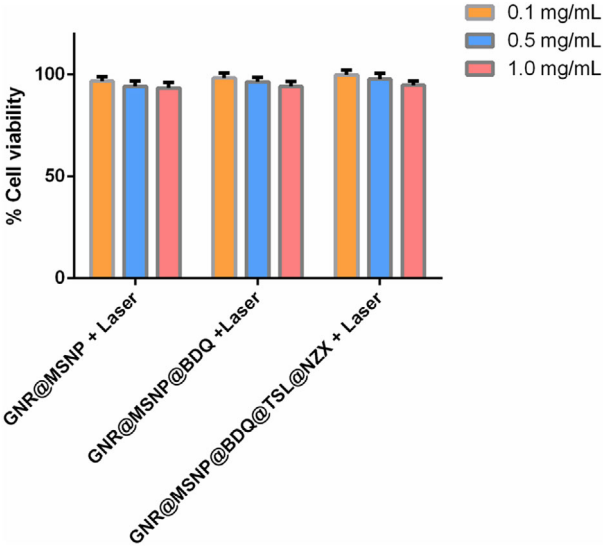

FIGURE 10 Percentage cell viability of A549 cells after incubation with different concentrations of irradiated nano-assemblies: GNR@MSNP, GNR@MSNP@BDQ and GNR@MSNP@BDQ@TSL@NZX after 24 hours

3 | CONCLUSION

In a post antibiotic era, novel therapeutic approaches have to be engineered to reduce the dependency on small molecule antibiotics. The GNR@MSNP@BDQ@TSL@NZX is a complex nano-assembly that is not only a drug delivery platform, but also a conduit for PTT. This multifaceted platform offers (1) synergistic therapy of small molecule antibiotic and PTT (2) targeted antibiotic delivery (3) NIR trigger release of antibiotics. The GNR@MSNP@BDQ@TSL@NZX were prepared by BDQ loading to GNR@MSNP and encapsulating within NZX tagged TSL. Upon irradiation with NIR laser, GNRs convert light into heat, causing melting of TSL, that induces the release of antibiotics. Targeting peptide NZX, guides the GNR@MSNP@BDQ@TSL@NZX to approach the bacterial cell surface. BDQ encapsulated in GNR@MSNP@BDQ@TSL@NZX was found to be 20-fold more efficacious compared to free drug equivalent. The final nano-assembly was capable of targeting and inhibiting 99.9% intracellular mycobacteria residing within A549 cells. This work provides proof-of-concept unique therapeutic approach to treat pathogenic infections and reduce the dependency on conventional antibiotics.

4 | EXPERIMENTAL SECTION

4.1 | Synthesis of GNRs

GNRs were fabricated via a seed method as described by El-Sayed et al., with some minor modifications.[36] CTAB coated seeds were prepared by chemical reduction of gold salt with $NaBH_4$. Briefly, a $HAuCl_4$ solution (0.25 mL, 0.01 M) was mixed with a CTAB solution (7.5 mL, 0.1 M) in a 25 mL round bottom flask under stirring. An ice-cold $NaBH_4$ solution (0.6 mL, 0.01 M) was injected quickly under vigorous stirring. The solution turned immediately brown yellow color, suggesting the formation of the gold seeds. The mixture was kept undisturbed at 30 °C for another 3-4 hours, to ensure the complete degradation of unreacted $NaBH_4$. All the solutions were prepared from stock solution in order to get reproducible results. The growth solution consisting of CTAB (600 mL, 0.1 M), $HAuCl_4$ (30 mL, 0.01 M), $AgNO_3$ (4.8 mL, 10 mM) and H_2SO_4 (12 mL, 0.5 M) was stirred together in a 1000 mL round-bottom flask. The growth solution was equilibrated at 30 °C while stirring for 10 minutes. Ascorbic acid (4.8 mL, 0.1 M) was injected into the growth solution quickly with vigorous stirring. The solution turned colorless immediately. Gold seeds (1.4 mL) were added and stirred for 5 minutes and then left to age overnight. The prepared GNRs were purified via two cycles of centrifugation at 12,000 rpm for 15 minutes and then re-dispersed into 150 mL of water for further modification. Materials and instruments were described in supporting information.

4.2 | Synthesis of GNR@MSNPs

GNR@MSNPs were synthesized according to the protocol developed by Matsuura *et. al.*, with some minor modifications.[37] First, 100 mL of purified GNRs were transferred into an aqueous solution of CTAB (500 mL, 0.8 mM) then the basicity of the solution was adjusted to pH 10-11 with NaOH (0.1 M). After equilibration at 30 °C for 10 minutes, a solution of TEOS/APTES/ethanol (400, 20, and 1380 µL, respectively, total 1.8 mL) was added into the mixture by three times injecting 0.6 mL with gentle stirring. The reaction mixture was allowed to react at 30 °C overnight. The synthesized GNR@MSNPs were centrifuged at 12,000 rpm for 15 minutes once and then re-dispersed in 120 mL of ethanolic NH_4NO_3 (0.75 mM) at 45 °C and kept overnight, to remove CTAB. The final GNR@MSNPs were purified by centrifugation (10000 rpm for 10 minutes) and re-dispersed in ethanol.

4.3 | RITC-labeled GNR@MSNPs

The RITC precursor was prepared in the following manner. RITC (8.0 mg, 0.015 mM in ethanol) was stirred overnight with APTMS (5.2 µL, 0.03 mM) in anhydrous ethanol (15.0 mL) at 42 °C to obtain the RITC-APTMS precursor. RITC-labeled GNR@MSNPs were synthesized via the same procedure as GNR@MSNPs except that the TEOS/APTES/ethanol solution was replaced by TEOS/APTES/RITC-APTMS/ ethanol solution (400, 20, and 1380 µL; total 1.8 mL) while the injected volume at each 30 minutes interval stayed the same. This reaction was performed in the dark.

4.4 | Surface area and pore volume determination of GNR@MSNPs

The surface area was determined using the Brunauer–Emmett–Teller (BET) model, Autosorb iQ-C-MP/XR (Quantachrome, USA) and the cumulative pore volume was calculated from the adsorption branch of the isotherm using the Barrette–Joyner–Halenda (BJH) model.

4.5 | Drug (BDQ) encapsulation in GNR@MSNPs

GNR@MSNPs (21 mg) were mixed with BDQ (7 mg) in 10 mL of DMSO while stirring overnight at 37 °C. The ratio of GNR@MSNPs and BDQ used in the entire study was 3:1 w/w (GNR@MSNPs 21 mg: BDQ 7 mg). The BDQ loaded GNR@MSNPs samples were collected by centrifugation at 10,000 rpm for 10 minutes, and vacuum dried to obtain dry powder. BDQ encapsulation efficiency and drug loading was determined by HPLC.

4.6 | Encapsulation of GNR@MSNP@BDQ in TSL

TSLs were prepared by a lipid film based method previously reported in the literature.[53] Briefly, DPPC (85% molar ratio), cholesterol (10% molar ratio) and DSPE-PEG2000 amine (5% molar ratio) were dissolved in 2 mL of $CHCl_3$ and evaporated in a rotary evaporator, yielding a thin lipid film. This thin lipid film was rehydrated in 10 mM HEPES buffer containing GNR@MSNP@BDQ (2 mg mL^{-1}) before extruded 15 times through two stacks of Nuclepore, Whatman polycarbonate membranes with a pore size of 800 nm (GE Healthcare, New York, USA) using a mini extruder set (Avanti Polar Lipids, Alabama, USA). The resultant nano-assembly (GNR@MSNP@BDQ@TSL) was stored at 4 °C until use.

4.7 | Conjugation of Msmeg targeting NZX peptide on TSL

GNR@MSNP@BDQ@TSL were conjugated with NZX, via EDC activation method; by activating the carboxyl group of the NZX peptide to react with the primary amines of DSPE-PEG2000 amine in the liposomes. NZX 0.1 mg mL^{-1} was dissolved in 0.1 M MES, 0.5 M NaCl, pH 6.0 (reaction buffer) and then activated with 10 fold molar excess of EDC (pH = 4.0) and 25 fold molar excess of sulfo-NHS for 30 minutes. Liposomes (GNR@MSNP@BDQ@TSL) were added to the reaction mixture and reacted for 24 hours at 37 °C. The molar ratio of NZX:liposome was maintained at 10:1. After 24 hours, the reaction mixture was purified by centrifugation at 10,000 rpm for 15 minutes at 25 °C to remove excess unreacted EDC.

4.8 | TGA analysis of various nano-assemblies of BDQ content in GNR@MSNPs

TGA was carried out under argon gas (99.999%) where dried GNR@MSNP@BDQ (~1 mg) was heated at rate of 5 °C min^{-1} to 100 °C and then kept isothermal at 100 °C for 15 minutes followed by 5 °C min^{-1} ramp to 700 °C. The BDQ loaded in GNR@MSNPs was calculated by analyzing the weight loss difference between GNR@MSNPs and GNR@MSNP@BDQ. Similarly, the TSL content was analyzed by measuring weight loss difference between GNR@MSNP@BDQ and GNR@MSNP@BDQ@TSL. Finally the amount of peptide was calculated by measuring weight loss difference between GNR@MSNP@BDQ@TSL and GNR@MSNP@BDQ@TSL@NZX.

4.9 | Analysis of colloidal stability

The stability of GNR@MSNP and liposome coated GNR@MSNP (GNR@MSNP@TSL) was conducted at 37 °C to mimic the static condition in an in vitro experiment. Nano-assemblies were dissolved in mammalian cell culture medium to a concentration of 1 mg mL^{-1} and incubated at 37 °C for 5 days.[54]

Kah et al., reported calculating an aggregation index (AI) as a stability parameter to determine the stability of GNRs.[45] AI is a measure of the LSPR peak broadening. This is calculated by dividing the total area under curve (AUC) of the absorbance spectra of GNR LSPR band from 600 to 900 nm, by the LSPR peak intensity (Equation 1).[45] AI calculates an equivalent bandwidth of longitudinal peak for a spectrum normalized to the LSPR peak intensity. The similar analysis was performed for GNR@MSNP and GNR@MSNP@TSL stability studies. The higher AI indicates, higher degree of aggregation, hence lower colloidal systems stability.[45,46]

$$\text{AI (nm)} = \frac{AUC\ of\ LSPR\ from\ 600-900\ nm}{LSPR\ peak\ intensity} \quad (1)$$

4.10 | NIR laser irradiation studies

The laser set up is explained in detail in supporting information Figure S1. Various weight concentrations ranging from 50, 100, 500 and 1000 μg mL^{-1} (calculated with respect to the weight of GNR@MSNPs) of the final nano-assemblies GNR@MSNP@BDQ@TSL@NZX were irradiated with the 808 nm NIR diode laser (500 mW) for a time period of 1-15 minutes. A digital thermocouple monitored the change in temperature.

4.11 | NIR laser triggered drug release

Final nano-assembly GNR@MSNP@BDQ@TSL@NZX was dispersed in 3 mL of release media (0.5% w/w SLS in 10 mM HEPES buffer, pH 7.2), then incubated at 37 °C with

constant agitation. At predetermined time intervals (2, 4, 6, 8, 12, 18, 24, 36, 48 and 72 hours), the suspension was exposed to the NIR laser (808 nm, 500 mW) for 15 minutes and then centrifuged at 15,000 rpm for 15 minutes, the supernatant collected and replaced with the same volume of fresh prewarmed (37 °C) release media. The pellet was resuspended in the new release media and further incubated. Each sampled aliquot of the supernatant was passed through a 0.22 μm nylon filter. Quantification of the drug release was performed by HPLC (equipped with UV detector): HPLC Hitachi Primaide separation module equipped with a 1430 diode array detector and a reverse phase SunFire C18 column. Elution was performed using a mobile phase composed of a linear gradient of ACN and TFA at 0.1% (v/v) in water. BDQ was eluted using linear gradient mode with 50:50 TFA:ACN for 2 minutes, 30:70 TFA:ACN 2.1 – 15.1 minutes and final column wash using 50:50 TFA:ACN ratio from 15.2 to 18 minutes. Injection volume was 20 μL and the absorbance was recorded at 230 nm. The operating temperature was 40 °C and the flow rate kept at 1.2 mL min^{-1}. Calibration curve for BDQ was generated using 1.0, 2.5, 5.0, 7.5 and 10.0 μg mL^{-1} of BDQ diluted in the release media release media: 0.5% w/v SLS containing 10 mM HEPES, pH 7.2 (Figure S2). To quantify the BDQ release without laser exposure, a similar experiment was conducted in absence of the NIR laser light exposure. The BDQ release from the final nano-assembly was quantified by HPLC.

4.12 | *Msmeg* culture and viability assays

Msmeg were routinely grown at 37 °C in Middlebrook 7H9 medium supplemented with 10% ADC and 0.05% glycerol. WST-8 cell viability assays were conducted using assay instructions. Briefly, in a flat bottom 96-well plate, 10 μL of *Msmeg* (10^8 CFU mL^{-1}), 170 μL of Middlebrook broth and an aliquot of 20 μL of various nano-assemblies added and shaken (2000 rpm) at 37 °C on a shaker bed for 24 hours. After 24 hours incubation, the bacterial viability was determined by a WST-8 assay. The absorbance was recorded at 450 nm using a plate reader. High absorbance at 450 nm was interpreted as higher viability of the bacterial cells. The viable count of bacteria in each well was quantified using standard spread plate methods followed by the colony counts. From each well, a volume of 10 μL was serially diluted and spread onto the nutrient agar plates and incubated at 37 °C for 24 hours. Agar plates with 30 to 300 colonies were counted and the viable bacteria were reported as CFU mL^{-1}.

4.13 | Antibacterial activity studies with and without laser exposure

The viability of bacteria treated with nano-assemblies with and without NIR laser (808 nm, 500 mW) exposure was determined by WST-8 cell viability assay and verified by the colony counting. Antibacterial activity of (a) GNR@MSNPs (b) GNR@MSNP@BDQ (c) final nano-assembly GNR@MSNP@BDQ@TSL@NZX (e) BDQ (f) NZX was determined by WST-8 assay and colony counts. Various sample concentrations of a-f from 0.01-1000 μg mL^{-1} were used and MIC of each material was determined. MIC is the minimum inhibitory concentration, that is, lowest concentration of drug that effectively inhibits growth of bacteria.

Furthermore, the antibacterial activity of the nano-assemblies with or without NIR laser exposure was analyzed by colony counts. The percentage viable count of bacteria treated with material in presence and absence of laser was calculated using following:

Equation 2

$$\%\ Reduction = \frac{Initial\left(\frac{CFU}{mL}\right) - Test\left(\frac{CFU}{mL}\right)}{Initial\left(\frac{CFU}{mL}\right)} \times 100\% \quad (2)$$

The initial colony count was kept at 10^8 CFU mL^{-1} and test count (CFU mL^{-1}) was obtained after treatment.

4.14 | Quantification of ROS

DCFH-DA was used as a fluorescent probe to assess the generation of ROS in bacteria. Briefly, 50 μL of *Msmeg* (10^8 CFU mL^{-1}) was incubated with 150 μL (1 mg mL^{-1} concentration) of GNR@MSNP@BDQ and final nano-assembly GNR@MSNP@BDQ@TSL@NZX for 4 hours. Bacteria alone is used as a negative control. After incubation all samples were exposed to NIR laser (808 nm, 500 mW) for 15 minutes. This was followed by addition of 100 μL of ROS reagent (DCFH-DA) and incubation for 1 hours. Fluorescent intensity was quantified at 525 nm, with excitation at 490 nm. Samples were also observed by fluorescence microscopy.

4.15 | Live/dead assay

To further investigate the antibacterial, PT effect and targeting capacity of the nano-assemblies, live/dead assay was conducted. In a flat bottom 96-well plate,

Msmeg (10^8 CFU mL^{-1}, 10 μL) was treated with BDQ, GNR@MSNP@BDQ and final nano-assembly GNR@MSNP@BDQ@TSL@NZX (1 mg mL^{-1}, 20 μL) and diluted with 170 μL of growth medium. After incubation for 3 hours (37 °C), the samples were irradiated with the NIR laser (808 nm, 500 mW) for 15 minutes. The supernatant was removed by centrifugation at 5000 rpm for 10 minutes and the pellet was washed 3x with HEPES. The bacteria treated with nano-assemblies were stained with SYTO 9 and propidium iodide (PI) for 30 minutes at 37 °C. Finally, the live and dead cells were examined under an inverted fluorescence microscope.

4.16 | A549 cell proliferation

A549 cells were grown in T75 flasks in complete growth medium. Complete growth medium was prepared by mixing Ham's F-12K nutrient mixture with L-glutamine (F-12K) (1X, 445 mL), FBS (10%, 50 mL) and Pen-Strep (1X, 5 mL) followed by sterile filtration. The cells were grown in 20 mL of fresh and prewarmed medium at 37 °C in a humidified atmosphere of 5% CO_2. Cells viability was assessed in trypan blue assay and cells counted through automatic cell counter.

4.17 | GNR@MSNP@BDQ@TSL@NZX uptake by A549 cells

In order to image the cellular uptake of the final nano-assembly GNR@MSNP@BDQ@TSL@NZX was labelled with the red fluorescent dye RITC. A549 cells (10^3 cells mL^{-1}) were cultured on a 24 well plate for 24 hours until complete adhesion occurs. After adhesion and confluence (~90%), A549 cells were incubated at 37 °C with RITC-GNR@MSNP@BDQ@TSL@NZX (50 μg mL^{-1}) for 0.5, 1.0, or 3.0 hours. The cells were washed 3x with cold PBS and followed by calcein AM (10 μM) and Hoechst dye (10 μM), staining for 30 minutes at 37 °C. The samples were analyzed through an inverted fluorescent microscope.

4.18 | Cellular uptake mechanism of nano-assemblies

A549 cells (10^3 cells mL^{-1}) were cultured on a 24 well plate for 24 hours until complete adhesion occurs and then pre-treated with different endocytosis inhibitors : chlorpromazine (20 μg mL^{-1}), nystatin 20 and wortmannin 1 μg mL^{-1} for 30 minutes. A549 cells were treated with 50 μg mL^{-1} GNR@MSNP@BDQ and GNR@MSNP@BDQ@TSL@NZX, then incubated for 2 hours at 37°C. An inverted fluorescent microscope used to qualitatively evaluate the uptake of the nano assemblies by lung cells. Increase in red fluorescence intensity within the lung cells is related to high uptake of nano-assemblies. To quantitatively determine cellular uptake of nano-assemblies, the lung cells (A549) were lysed with 0.5% Triton X-100 in the presence of 0.2 M NaOH. Fluorescence microplate reader was used to measure the fluorescence intensity at excitation and emission wavelengths of 544 and 576 nm, which corresponds to excitation and emission of RITC. Fluorescence intensity of the lysed samples was measured. Fluorescence intensity of the controls (without inhibitor) was set as 100%. The reduction fluorescence intensity of the samples (with inhibitor) was measured in comparison to the control.

4.19 | Determination of intracellular antibacterial activity of nano-assemblies

A549 cells (10^3 cells mL^{-1}) were seeded in a 24 well plate and incubated overnight in a 5% CO_2 at 37 °C. An aliquot of 5 μL *Msmeg* (17×10^4 CFU mL^{-1}) was added per well of A549 cells and incubated for 30 minutes at 37 °C. After incubation, the supernatant was discarded, and the infected cells were washed twice with PBS (1X). Then the mammalian cell culture medium was replaced with a medium supplemented with 30 μg mL^{-1} BDQ to kill the remaining extracellular bacteria without affecting the intracellular bacteria. The infected A549 cells were treated with 50 μg mL^{-1} of GNR@MSNP@BDQ and GNR@MSNP@BDQ@TSL@NZX then exposed to NIR laser (808 nm, 500 mW, 15 minutes) and incubated for additional 24 hours. After overnight incubation, the cells stained with calcein AM (10 μM) and Hoechst dye (10 μM), for 30 minutes at 37 °C. The samples were analyzed through a confocal fluorescent microscopy. Finally, A549 cells were lysed in distilled water for 3 hours. The cell lysate was plated on agar and the bacterial colonies were quantified. The number of colonies reflects the viable intracellular *Msmeg* present after treatment.

4.20 | Mammalian cell viability assays

Cell viability was evaluated by using MTT assay. A549 cells were seeded onto 24 well plate at a density of 1×10^3 cells $well^{-1}$ (1 mL per well). After reaching 90% confluence, they were treated with various concentration (1.0, 0.5, and 0.1 mg mL^{-1}) of GNR@MSNPs, GNR@MSNP@BDQ and final nano-assembly GNR@MSNP@BDQ@TSL@NZX. Treated cells were exposed to NIR laser 808 nm, 500 mW for 15 minutes. Finally, 10 μL of the MTT solution

(1 mg mL^{-1}) was added into each well, and the cells were further incubated for 4 hours. After incubation, the supernatant was discarded and 150 μL of DMSO was added into each well. The absorbance intensity was determined at 590 nm by a microplate reader. Results were presented as the percentage (%) with respect to untreated control A549 cells.

ACKNOWLEDGMENTS

The authors thank VINSE facility Vanderbilt University for allowing us to use TEM, Dr. Yu Lei for giving access to the BET instrument for porosity analysis and Prof. Carmen Scholz and Prof. L. John Foster for kindly reviewing our manuscripts before submission. Internal awards of The University of Alabama in Huntsville funded this work.

CONFLICT OF INTEREST

The authors declare no conflicts of interests.

DATA AVAILABILITY STATEMENT

Research data are not shared.

ORCID

Unnati Patel https://orcid.org/0000-0002-5117-2094
Surangi N. Jayawardena https://orcid.org/0000-0001-5866-9346

REFERENCES

1. CDC., *Antibiotic Resistance Threats in the United States*, U.S. Department of Health and Human Services: Atlanta, GA, **2019**.
2. X. Zhu, A. F. Radovic-Moreno, J. Wu, R. Langer, J. Shi, *Nano Today* **2014**, *9*, 478.
3. B. Kuehn, *JAMA, J. Am. Med. Assoc.* **2019**, *322*, 2376.
4. X. Y. Wong, A. Sena-Torralba, R. Álvarez-Diduk, K. Muthoosamy, A. Merkoçi, *ACS Nano* **2020**, *14*, 2585.
5. G. Qing, X. Zhao, N. Gong, J. Chen, X. Li, Y. Gan, Y. Wang, Z. Zhang, Y. Zhang, W. Guo, Y. Luo, X.-J. Liang, *Nat. Commun.* **2019**, *10*, 4336.
6. I. Altinbasak, R. Jijie, A. Barras, B. Golba, R. Sanyal, J. Bouckaert, D. Drider, R. Bilyy, T. Dumych, S. Paryzhak, V. Vovk, R. Boukherroub, A. Sanyal, S. Szunerits, *ACS Appl. Mater. Interfaces* **2018**, *10*, 41098.
7. H. Wang, Z. Song, S. Li, Y. Wu, H. Han, *ACS Appl. Mater. Interfaces* **2019**, *11*, 32659.
8. M. Harris, H. Ahmed, B. Barr, D. LeVine, L. Pace, A. Mohapatra, B. Morshed, J. D. Bumgardner, J. A. Jennings, *Int. J. Biol. Macromol.* **2017**, *104*, 1407.
9. C. Xu, O. U. Akakuru, J. Zheng, A. Wu, *Frontiers in bioengineering and biotechnology* **2019**, *7*.
10. Y. Yao, Y. Wang, F. Huang, *Chem. Sci.* **2014**, *5*, 4312.
11. D. Wu, X. Chen, J. Zhou, Y. Chen, T. Wan, Y. Wang, A. Lin, Y. Ruan, Z. Chen, X. Song, W. Fang, H. Duan, Y. Ping, *Mater. Horiz.* **2020**, *7*, 2929.
12. J. G. Piao, L. Wang, F. Gao, Y. Z. You, Y. Xiong, L. Yang, *ACS Nano* **2014**, *8*, 10414.
13. U. S. Chung, J.-H. Kim, B. Kim, E. Kim, W.-D. Jang, W.-G. Koh, *Chem. Commun.* **2016**, *52*, 1258.
14. M. Wang, Y. Liu, X. Zhang, L. Luo, L. Li, S. Xing, Y. He, W. Cao, R. Zhu, D. Gao, *J. Mater. Chem. B* **2017**, *5*, 2161.
15. J. Nam, S. Son, L. J. Ochyl, R. Kuai, A. Schwendeman, J. J. Moon, *Nat. Commun.* **2018**, *9*, 1074.
16. P. Li, Y. Wu, D. Li, X. Su, C. Luo, Y. Wang, J. Hu, G. Li, H. Jiang, W. Zhang, *Nanoscale Res. Lett.* **2018**, *13*, 313.
17. Y.-H. Chien, K. K. Chan, T. Anderson, K. V. Kong, B. K. Ng, K.-T. Yong, *Advanced Therapeutics* **2019**, *2*, 1800090.
18. Z. Jiang, B. Dong, B. Chen, J. Wang, L. Xu, S. Zhang, H. Song, *Small* **2013**, *9*, 604.
19. G.-F. Luo, W.-H. Chen, Q. Lei, W.-X. Qiu, Y.-X. Liu, Y.-J. Cheng, X.-Z. Zhang, *Adv. Funct. Mater.* **2016**, *26*, 4339.
20. K. Rathnayake, U. Patel, C. Pham, A. McAlpin, T. Budisalich, S. N. Jayawardena, *ACS Appl. Bio Mater.* **2020**, *3*, 6708.
21. L. Chen, M. Liu, Q. Zhou, X. Li, *Emergent Materials* **2020**, *3*, 381.
22. H. S. N. Jayawardena, S. H. Liyanage, K. Rathnayake, U. Patel, M. Yan, *Anal. Chem.* **2021**, *93*, 1889.
23. C. Zylberberg, S. Matosevic, *Drug Delivery* **2016**, *23*, 3319.
24. In *Drug Delivery*, **2016**, pp 272-298.
25. J.-W. Xu, K. Yao, Z.-K. Xu, *Nanoscale* **2019**, *11*, 8680.
26. E. Tenland, N. Krishnan, A. Rönnholm, S. Kalsum, M. Puthia, M. Mörgelin, M. Davoudi, M. Otrocka, N. Alaridah, I. Glegola-Madejska, E. Sturegård, A. Schmidtchen, M. Lerm, B. D. Robertson, G. Godaly, *Tuberculosis* **2018**, *113*, 231.
27. H. Jenssen, P. Hamill, R. E. W. Hancock, *Clin. Microbiol. Rev.* **2006**, *19*, 491.
28. W.-L. Chiang, T.-T. Lin, R. Sureshbabu, W.-T. Chia, H.-C. Hsiao, H.-Y. Liu, C.-M. Yang, H.-W. Sung, *J. Controlled Release* **2015**, *199*, 53.
29. D. Hu, L. Zou, B. Li, M. Hu, W. Ye, J. Ji, *ACS Biomater. Sci. Eng.* **2019**, *5*, 5169.
30. K. Ma, Y. Li, Z. Wang, Y. Chen, X. Zhang, C. Chen, H. Yu, J. Huang, Z. Yang, X. Wang, Z. Wang, *ACS Appl. Mater. Interfaces* **2019**, *11*, 29630.
31. *Global tuberculosis report*. **2020**.: Geneva: World Health Organization, 2020.
32. C. Bussi, M. G. Gutierrez, *FEMS Microbiol. Rev.* **2019**, *43*, 341.
33. E. Tenland, A. Pochert, N. Krishnan, K. Umashankar Rao, S. Kalsum, K. Braun, I. Glegola-Madejska, M. Lerm, B. D. Robertson, M. Lindén, G. Godaly, *PLoS One* **2019**, *14*, e0212858.
34. H. R. Ali, M. R. K. Ali, Y. Wu, S. A. Selim, H. F. M. Abdelaal, E. A. Nasr, M. A. El-Sayed, *Bioconjugate Chem.* **2016**, *27*, 2486.
35. B. Li, Q. Tan, Z. Fan, K. Xiao, Y. Liao, *Advanced Therapeutics* **2020**, *3*, 1900189.
36. B. Nikoobakht, M. A. El-Sayed, *Chem. Mater.* **2003**, *15*, 1957.
37. I. Gorelikov, N. Matsuura, *Nano Lett.* **2008**, *8*, 369.
38. J. Liu, C. Detrembleur, M. C. De Pauw-Gillet, S. Mornet, C. Jérôme, E. Duguet, *Small* **2015**, *11*, 2323.
39. S. Yang, X. Han, Y. Yang, H. Qiao, Z. Yu, Y. Liu, J. Wang, T. Tang, *ACS Appl. Mater. Interfaces* **2018**, *10*, 14299.
40. T. L. Moore, L. Rodriguez-Lorenzo, V. Hirsch, S. Balog, D. Urban, C. Jud, B. Rothen-Rutishauser, M. Lattuada, A. Petri-Fink, *Chem. Soc. Rev.* **2015**, *44*, 6287.
41. P. K. Jain, M. A. El-Sayed, *Chem. Phys. Lett.* **2010**, *487*, 153.
42. E. Hao, S. Li, R. C. Bailey, S. Zou, G. C. Schatz, J. T. Hupp, *J. Phys. Chem. B* **2004**, *108*, 1224.

43. R. Chapman, Y. Lin, M. Burnapp, A. Bentham, D. Hillier, A. Zabron, S. Khan, M. Tyreman, M. M. Stevens, *ACS Nano* **2015**, *9*, 2565.
44. A. Albanese, W. C. Chan, *ACS Nano* **2011**, *5*, 5478.
45. J. C. Y. Kah, A. Zubieta, R. A. Saavedra, K. Hamad-Schifferli, *Langmuir* **2012**, *28*, 8834.
46. X. Du, W.-C. Lin, Q. Shou, X. Liang, H. Liu, *Colloid Polym. Sci.* **2019**, *297*, 891.
47. H. Bi, J. Xue, H. Jiang, S. Gao, D. Yang, Y. Fang, K. Shi, *Asian J. Pharm. Sci.* **2019**, *14*, 365.
48. K. Chamchoy, D. Pakotiprapha, P. Pumirat, U. Leartsakulpanich, U. Boonyuen, *BMC Biochem.* **2019**, *20*, 4.
49. F.-L. Mi, T. Burnouf, S.-Y. Lu, Y.-J. Lu, K.-Y. Lu, Y.-C. Ho, C.-Y. Kuo, E.-Y. Chuang, *Adv. Healthcare Mater.* **2017**, *6*, 1700181.
50. S. Yougbaré, C. Mutalik, D. I. Krisnawati, H. Kristanto, A. Jazidie, M. Nuh, T.-M. Cheng, T.-R. Kuo, *Nanomaterials* **2020**, *10*, 1123.
51. A. Sikder, J. Sarkar, R. Barman, S. Ghosh, *J. Phys. Chem. B* **2019**, *123*, 7169.
52. S. Behzadi, V. Serpooshan, W. Tao, M. A. Hamaly, M. Y. Alkawareek, E. C. Dreaden, D. Brown, A. M. Alkilany, O. C. Farokhzad, M. Mahmoudi, *Chem. Soc. Rev.* **2017**, *46*, 4218.
53. X. Cui, W. Cheng, X. Han, *J. Mater. Chem. B* **2018**, *6*, 8078.
54. A. Y. Deneka, Y. Boumber, T. Beck, E. A. Golemis, *Cancers* **2019**, *11*, 1297.

SUPPORTING INFORMATION

Additional supporting information may be found online in the Supporting Information section at the end of the article.

How to cite this article: Patel U, Rathnayake K, Jani H, et al. Near-infrared responsive targeted drug delivery system that offer chemo-photothermal therapy against bacterial infection. *Nano Select*. 2021;1–20. https://doi.org/10.1002/nano.202000271